Nuclear Inst. and Methods in Physics Research, A 960 (2020) 163665

Contents lists available at ScienceDirect

Nuclear Inst. and Methods in Physics Research, A

journal homepage: www.elsevier.com/locate/nima

Detector response of Cherenkov radiators for calorimetry in the energy range below 14 MeV

M. Christmann [a,b,1], P.F. Burger [a,b,2], P. Achenbach [a,b,c,*], S. Aulenbacher [a], M. Ball [d], S. Baunack [a,b], J.C. Bernauer [e], M. Biroth [a], P. Brand [f], S. Caiazza [a], E. Cline [e], A. Denig [a,b,c], L. Doria [a,c], I. Friščić [g], J. Geimer [a], P. Gülker [a], A. Khoukaz [f], M. Kohl [h], T. Kolar [i,j], M. Lauß [a], W. Lauth [a], M. Littich [a], M. Lupberger [d], S. Lunkenheimer [a], F.E. Maas [a,b,c], M. Mauch [a], H. Merkel [a,c], M. Mihovilovič [i,j], R.G. Milner [g], J. Müller [a], J. Rausch [a], B.S. Schlimme [a], C. Sfienti [a,c], S. Širca [i,j], S. Stengel [a], C. Szyszka [a], S. Vestrick [f], Y. Wang [g]

[a] Institut für Kernphysik, Johannes Gutenberg-Universität, 55099 Mainz, Germany
[b] Helmholtz-Institut Mainz, Johannes Gutenberg-Universität, 55099 Mainz, Germany
[c] PRISMA$^+$ Cluster of Excellence, Johannes Gutenberg-Universität, 55099 Mainz, Germany
[d] Helmholtz-Institut für Strahlen- und Kernphysik, Rheinische Friedrich-Wilhelms-Universität Bonn, 53115 Bonn, Germany
[e] College of Arts and Sciences, Stony Brook University, NY 11794-3391, USA
[f] Institut für Kernphysik, Westfälische Wilhelms-Universität Münster, 48149 Münster, Germany
[g] Laboratory for Nuclear Science, Massachusetts Institute of Technology, Cambridge, MA 02139, USA
[h] Department of Physics, Hampton University, Hampton, VA 23668, USA
[i] Department of Physics, University of Ljubljana, 1000 Ljubljana, Slovenia
[j] Jožef Stefan Institute, 1000 Ljubljana, Slovenia

ARTICLE INFO

Keywords:
Cherenkov light detector
Lead fluoride
Lead glass
Light yield
Optical transmittance
Electromagnetic calorimetry

ABSTRACT

A study of the detector response of PbF_2 crystals and three different types of lead glass blocks to electrons from a 14-MeV beam of the Mainz Microtron MAMI is presented. For the first time, signal height, signal width, and homogeneity of the response of these Cherenkov radiators were determined for energies between 10 and 14 MeV. To complement the beam tests, optical properties of the materials, in particular measured transmittances in the near UV and visible spectrum, were studied. The measured detector responses were also compared to Monte Carlo simulations of energy-loss, light production, transport, and detection. These Cherenkov radiators are considered as active material of a low-energy calorimeter for the detection of light dark matter particles recoiling off electrons behind the beam-dump of the Mainz Energy Recovering Superconducting Accelerator MESA.

1. Introduction

At the Johannes Gutenberg Universität in Mainz, the Mainz Energy Recovering Superconducting Accelerator (MESA) is currently under construction. The electron beam-dump experiment at MESA (DarkMESA) has a powerful discovery potential for dark sector particles in the light mass range [1,2]. The possible existence of such light dark matter (LDM) is a candidate explanation for the long-standing dark matter problem [3].

With 10 000 h of operation time scheduled for the P2 experiment at MESA [4], the dump of the external 150 μA beam with 150 MeV energy could act as a strong source of LDM. These particles would be produced copiously in the relativistic electron–nucleus collisions if they were coupling to electrons via vector mediators, called dark photons. After production, they could be detected within the shielded DarkMESA setup down-stream of the dump.

The sensitive detector part of DarkMESA will be constructed from total absorbing calorimeters to detect the transferred energy in elastic scattering of LDM particles off electrons, which is dependent on scattering angle and mass. A general feature of the recoil energy distributions is their peaking towards low energies. The electronic recoil energy distribution extends from a few MeV up to nearly the kinetic energy of the LDM particles. The latter can reach half the electron beam energy for small LDM and dark photon masses. In contrast, the nuclear recoil

* Corresponding author at: Institut für Kernphysik, Johannes Gutenberg-Universität, 55099 Mainz, Germany.
E-mail address: achenbach@uni-mainz.de (P. Achenbach).
[1] Part of doctoral thesis.
[2] Part of bachelor thesis.

https://doi.org/10.1016/j.nima.2020.163665
Received 5 November 2019; Received in revised form 11 February 2020; Accepted 15 February 2020
Available online 18 February 2020
0168-9002/

Table 1
Properties of calorimeter materials that were considered in the design studies for the DarkMESA detector. Note that the light yield is dependent on the optical quality and the light collection efficiency of the detectors as well as the coupling and quantum efficiency of the photo-sensors. The peak wavelength in the emission spectrum of Cherenkov radiators depends on the transmittance of the material. More details on different PbGl types are given in Table 2.

Material	CsI(Tl)	PbF_2	BGO	PbGl
Type	BaBar endcap	A4 ring	L3 endcap	various
Cross-section (cm^2)	4.7^2–6.0^2	2.6^2–3^2	2.1^2	$\sim 3^2$
Length (cm)	32.5	15–18	23	15
Shape of blocks	tapered	tapered	cuboid	cuboid
Density (g/cm^3)	4.53	7.77	7.13	3.6–5.5
Radiation length (cm)	1.85	0.93	1.13	1.6–3.2
Light yield (ph./MeV)	50 000	~25	10 000	~15
Signal height (p.e./MeV)	7600	~2	1200	~1
Peak emission (nm)	565	350	480	~450
Signal decay time (ns)	680 (64%) 3340 (36%)	prompt	300	prompt
Refractive index	1.80	1.7–1.9	2.19	1.6–1.9
References	[6,7]	[12,14]	[8,9]	[12,13]

energy is too low to be detected. At the lowest energies, background from the environment or of cosmic origin will dominate, so that an energy region with especially high LDM detection sensitivity is located near 10 MeV. In order to experimentally establish the anticipated performance of scintillating or Cherenkov light calorimeters, measurements of detector responses over a range of electron energies relevant for LDM detection were performed.

2. Studied calorimeter materials

The choice of the detector material for the DarkMESA calorimeters will depend on volume, density, granularity, backgrounds, energy resolution, energy threshold for signal detection, and costs. Lead tungstate, $PbWO_4$ (PWO), is one of the most widely used inorganic scintillation materials in electromagnetic calorimetry in modern accelerator experiments. With a density of 8.3 g/cm^3 and a large lead content it has one of the shortest radiation lengths, $X_0 = 0.89$ cm, of all calorimeter materials. The complex scintillation mechanism has a fast decay time, but low light output [5]. CsI(Tl) and BGO are inorganic scintillators with higher light yields and lower densities [6–9]. At the Thomas Jefferson Laboratory (JLab) in the United States a complementary search for LDM is planned (BDX@JLab), for which several hundred CsI(Tl) crystals from the former BaBar experiment are available [10]. A completely different approach was taken at the Laboratori Nazionali di Frascati (LNF) in Italy by the PADME experiment which is performing a dark photon search using the missing mass technique in a positron beam on a diamond target. The active volume is composed by more than 600 BGO crystals from a dismantled endcap of the former L3 experiment at CERN [11].

Advantages of high-density Cherenkov radiators compared to inorganic scintillators are their short response time, directionality, and lower sensitivity to background neutrons. A relevant disadvantage is their lower light yield. A typical Cherenkov radiator with a high lead content is lead glass (PbGl). PbGl comes in different types that show a large variation in density and optical properties, a commonly used type is SF5 [12,13]. PbF_2 is an extremely compact Cherenkov radiator with a radiation length X_0 of only 37% of the one of SF5 [12]. Table 1 lists properties of different calorimeter materials considered for the DarkMESA detector. In the following, details of the studied Cherenkov radiators PbF_2 and PbGl are presented.

2.1. PbF_2

Lead fluoride in the cubic lattice structure (β-PbF_2) is available for electromagnetic calorimetry in form of large and transparent monocrystals. The advantages of PbF_2 as an active calorimeter material are its high density ρ of 7.77 g/cm^3, its short radiation length X_0 of only 0.93 cm, its small Molière radius R_M of 2.2 cm (apparent $R_M \approx 1.8$ cm for Cherenkov light production [12]) and its high optical transmittance extending below 270 nm.

Since the 1990s, the A4 Collaboration has developed and operated the largest PbF_2 calorimeter worldwide [14–16] at the Mainz Microtron (MAMI) [17]. It consisted of 1022 individual crystals arranged in seven rings to form a total absorbing homogeneous barrel for the detection of electrons of several hundred MeV energy. The crystals have the geometry of pyramidal sectors with trapezoidal basis. Their average cross-section is 26 × 26 mm^2 at the front face and 30 × 30 mm^2 at the rear face and their lengths vary between 150.0 and 185.4 mm, corresponding to $16 - 20\ X_0$.

PbF_2 is currently used as electromagnetic calorimeter material for the new muon ($g - 2$) experiment at the Fermi National Accelerator Laboratory in the United States [18], and as forward bremsstrahlung photon calorimeter in a 5 × 5 matrix (Small-Angle Calorimeter) of the PADME experiment at LNF [11,19].

Table 2
Properties of three different types of PbGl that are available from Schott [20] and that were studied in the electron beam-tests at MAMI. The internal transmittances are given for a sample thickness of 25 mm.

Material	SF5	SF6	SF57HTU
Length of blocks (cm)	15.05	14.95	15.05
Cross-section of blocks (cm^2)	3.28 × 3.35	3.15 × 2.93	2.98 × 2.95
Shape of blocks	Cuboid	Cuboid	Cuboid
Density (g/cm^3)	4.07	5.18	5.51
Radiation length (cm)	2.55	1.70	1.55
Refractive index @ 405 nm	1.71	1.86	1.91
Internal transmittance @ 405 nm (%)	96	84	86

2.2. Lead glasses

A large number of PbGl types for electromagnetic calorimetry exist. They are chemically composed of a mixture of PbO and SiO_2 with a low fraction of alkali metal oxides. The properties of three different types (SF5, SF6, and SF57HTultra) [20] which are available from Schott AG, Mainz, are listed in Table 2. The PbO content in all of them is above 50% by weight and is largest for SF57 (74.8%), followed by SF6 (61%) and SF5 (51%). The change in PbO content is reflected in the variation of densities, radiation lengths, transmission edges, and refractive indices. The lower transmission edge of SF5 makes it well suited as Cherenkov radiator. To our knowledge, it is for the first time that the ultra-high transparent material SF57HTultra, with improved transmittance especially in the blue to violet spectral range, is studied as a possible electromagnetic calorimeter material.

3. Optical properties of the calorimeter materials

The light yield of pure Cherenkov radiators is low when compared to scintillating plastics or inorganic crystals and the spectrum of generated Cherenkov photons is peaked toward short wavelengths. Therefore, it is important that a high transmittance extends to wavelengths below 400 nm where the refractive index diverges. The number of detectable photoelectrons (p.e.), $N_{p.e.}$, is given by

$$\frac{d^2 N_{p.e.}}{d\lambda dx} = \frac{2\pi\alpha}{\lambda^2}\left(1 - \frac{1}{\beta^2 n^2(\lambda)}\right)\rho(\lambda)\,\tau_i(\lambda)\,t(\lambda), \quad (1)$$

where $\rho(\lambda)$ is the quantum efficiency of the photo-sensor, $\tau_i(\lambda)$ the internal transmittance of the material, $t(\lambda)$ the transmission factor between radiator and sensor, and x the radiator thickness. The transmittance and the refractive index are the two relevant optical properties of the radiator in terms of light yield and energy threshold, which define the energy resolution of a Cherenkov light calorimeter.

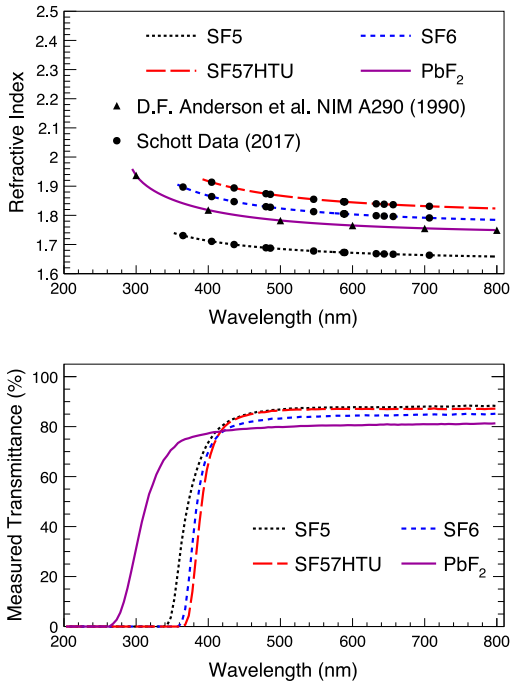

Fig. 1. Top: Comparison of the refractive indices of PbF_2 [12,21] and three different lead glasses [20] in the near UV and optical spectrum parameterized using a Sellmeier formula. The parameters for multiple absorption resonances are given in Table 3. Bottom: Comparison of transmittances measured along the longitudinal axis of representative samples. The corresponding internal transmittances and absorption lengths are given in Appendices A and B.

The optical quality of Cherenkov radiators can be characterized by their light absorption lengths $\Lambda_{\text{abs}} = -x/\ln(\tau_i)$ that can be determined from the internal transmittance $\tau_i = \exp(-x/\Lambda_{\text{abs}})$, where x the sample thickness. Note that an internal transmittance τ of 100% results in an external, measurable transmittance of typically below 90% because of reflections at the air–sample interfaces.

The external transmittances of different samples have been measured with the commercial spectrophotometer Shimadzu UV-2101 PC in double beam mode that utilizes two beams of light, a reference beam and a sampling beam that passes through the sample in a large sample compartment. The detector system was equipped with a light integrating sphere. A comparison of measured transmittances for representative samples of Cherenkov radiators is shown in Fig. 1.

The measured transmittances were corrected for the reflection losses using the Fresnel reflectivity for a light beam with normal incidence, irrespective of polarization: $R = (1-n)^2/(1+n)^2$. The reflection factor P representing the maximal external transmittance for a measurement with reflection losses at the front face and the rear face of the sample is then $P = (1-R)^2 = (4n)^2/(1+n)^4$. When considering an infinite series of reflections between parallel interfaces, the reflection factor gets larger:

$$P = (1-R)^2 + R^2(1-R)^2 + \cdots = \frac{1-R}{1+R} = \frac{2n}{1+n^2}\,. \tag{2}$$

For the transmittance spectra from the Cherenkov radiators considered in this study the difference of the reflection factor including reflections to the one neglecting reflections is smaller than one percent. A complete treatment would require the correction for absorption losses of the reflected light inside the sample which changes the reflection factor to

$$P = \frac{(4n)^2}{(1+n)^4 - (n-1)^4\exp(-2x/\Lambda_{\text{abs}})}\,. \tag{3}$$

However, this correction is on the level of 10^{-4} and was neglected.

The refractive indices show normal dispersion, $dn/d\lambda < 0$, and can be parameterized using a Sellmeier formula for multiple absorption resonances:

$$n^2(\lambda) = 1 + \sum_i \frac{B_i\lambda^2}{\lambda^2 - C_i^2} \tag{4}$$

Table 3
Parameterization of the refractive indices of PbF_2 [21] and three different lead glasses [20] in the near UV and optical spectrum using a Sellmeier formula for multiple absorption resonances: $n^2(\lambda) = 1 + \sum_i B_i\lambda^2/(\lambda^2 - C_i^2)$.

Material	B_1	C_1 (μm)	B_2	C_2 (μm)	B_3	C_3 (μm)	B_4	C_4 (μm)
PbF_2	0.67	3×10^{-4}	1.31	0.17	0.02	0.28	2008	796.67
SF5	1.46	0.01	0.25	0.05	0.95	112.04	–	–
SF6	1.72	0.01	0.39	0.06	1.05	119.56	–	–
SF57HTU	1.82	0.01	0.43	0.06	1.07	121.42	–	–

The parameters for PbF_2 and the three different types of PbGl are given in Table 3. The refractive indices in the near UV and optical spectrum are shown in Fig. 1.

The internal transmittance was then obtained by applying the formula $\tau_i = \tau/P$, from the internal transmittance the absorption length could finally be determined. These spectra are shown in Appendices A and B.

The different Cherenkov radiators were also studied by an optical simulation using `Geant4` version 10.4. and its internal optical transport routine. The optical description of the detectors included the experimentally determined transmittance spectra, the wavelength-dependent quantum efficiency of the PMTs, an reflective aluminum foil covering the active material, and an air gap. Signal noise and backgrounds were not included at this point. The beam-tests of the calorimeter prototypes were also simulated using the standard approach of describing the beam, materials in the setup, relevant interactions, and the energy-losses of all relevant particles.

4. Electron beam-tests of calorimeter prototypes

4.1. Experimental set-up

In order to establish the anticipated performance of the Cherenkov radiators experimentally it was necessary to carry out measurements over a range of energies relevant for the dark matter detection with DarkMESA. The detector responses of two PbF_2 crystals (from the A4 experiment at MAMI), two BGO crystals (from the L3 experiment at CERN, now at Frascati), and three different types (SF5, SF6, and SF57HTultra) of PbGl (from Schott, Mainz) have been determined with electrons from a 14-MeV beam of the racetrack microtron RTM1 at MAMI.

Fig. 2 shows a photograph and the schematics of the experimental setup. An array of six detectors was mounted on a remotely steerable table so that different beam positions and different incident angles of the beam could be realized.

All detectors were coupled to Philips XP2900/2901 photomultipliers (PMTs) with 1 1/8″ active diameter. Their bi-alkali photocathode has a maximum quantum efficiency at 420 nm and the transmittance of the borosilicate corning 801-51 window extends below 300 nm, which matches the light spectrum of the radiators. The PMTs were selected for a minimal cathode corning blue sensitivity of 11 μA/lm and a white sensitivity of 90 μA/lm. A 16-channel dual-range QDC of type V965 from CAEN was used to acquire the charge spectra with 12-bit resolution and a conversion of 200 fC per channel in the high-gain mode.

The data acquisition was triggered by a position sensitive detector in front of the calorimeter prototypes with a flexible active trigger area (region-of-interest) from 0.8×0.8 mm^2 to 13.3×13.3 mm^2. This detector was made from plastic scintillating fibers of 0.83 mm diameter in two layers for one direction and two further layers in the perpendicular direction. The average thickness of the detector was 2.4 mm corresponding to an energy-loss of 0.5 MeV for the beam.

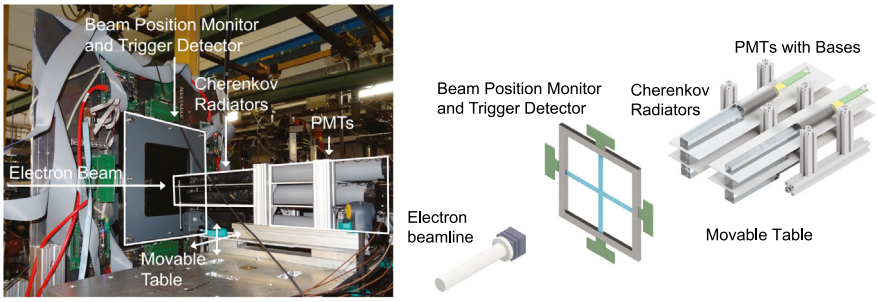

Fig. 2. Left: Photograph of the experimental setup used for the beam tests of calorimeter prototypes at MAMI. The electron beam entered from the left and the beam electrons were localized with a position sensitive detector that also provided the trigger signal to read out the prototype detectors. An array of six of such detectors was arranged on a remotely steerable table to realize different beam positions and different incident angles of the beam. Right: Schematics of the setup showing the relative positions of beam exit, energy degraders, crossed fiber layers, and prototype detectors.

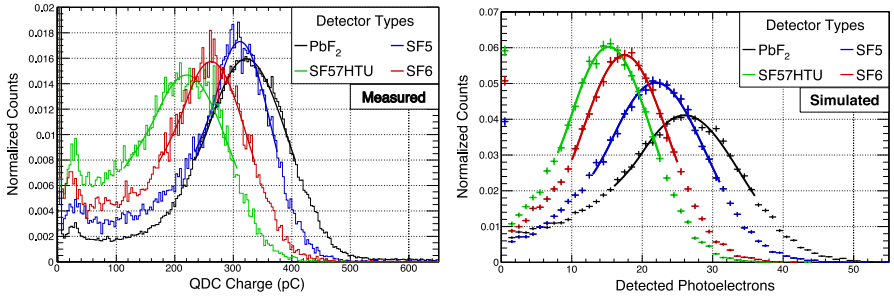

Fig. 3. Measured (left) and simulated (right) signals from three different types of PbGl detectors and a PbF_2 detector for a 14-MeV electron beam entering the front face of the radiators. The signal peaks were fitted with the Crystal Ball function.

The intrinsic energy spread of the MAMI beam is $\sigma_B \leq 0.01$ MeV. However, the beam left the vacuum beam pipe through an aluminum flange of 0.2 mm thickness and traversed ~300 mm of air before hitting the detectors. The resulting energy spread of the beam was simulated to be 0.07–0.08 MeV corresponding to a relative beam energy spread of $\sigma_B/E_B \approx 0.5\%$. The beam energy variation for different detector setups with different path lengths through air or detector material was found to be small. The multiple scattering in the flange increased the divergence of the 14-MeV beam to $\theta_B \approx 46$ mrad and the simulation predicted a beam spot of approximately $x_B \approx 17$ mm width (FWHM $\varnothing_B \approx 41$ mm) at the position of the detectors.

4.2. Signal fitting

The asymmetric distributions of the signals q in the spectra were fitted with the Crystal Ball function, which has a Gaussian part to describe the peak region and a power-law part on the low-energy side of the peak:

$$f(q;\alpha,n,E,\sigma_E) = \begin{cases} \exp(-\frac{(q-E)^2}{2\sigma_E^2}), & \text{for } \frac{q-E}{\sigma_E} > -\alpha \\ A\cdot(B-\frac{q-E}{\sigma_E})^{-n}, & \text{for } \frac{q-E}{\sigma_E} \leqslant -\alpha \end{cases} \quad (5)$$

with $A = (n/|\alpha|)^n \cdot \exp(-|\alpha|^2/2)$ and $B = n/|\alpha| - |\alpha|$, where α, n, E, and σ_E are parameters which were fitted to the data. The relative peak width σ_E/E was determined by the width of the Gaussian component. In the measured spectra, noise was present near the pedestal at $q <$ 50 pC corresponding to signals of 1–2 p.e. By limiting the fit range, the noise at small charges did not affect the extraction of the fit parameters. The uncertainties in the parameters originating from the fit were in general smaller than 1 pC.

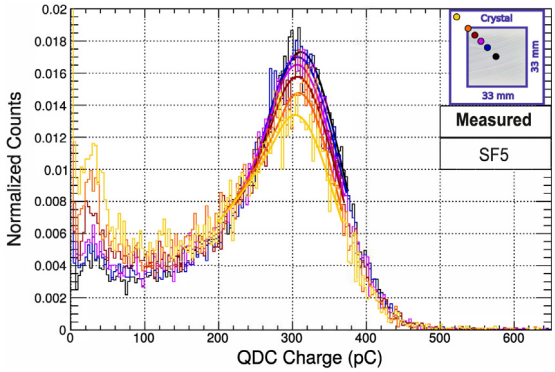

Fig. 4. Measured signals from a PbGl detector of type SF5 for a 14-MeV electron beam entering the front face of the radiator at different positions with respect to the center as indicated in the insert. The FWHM of the beam was $\varnothing_B \approx 41$ mm. The signal peaks were fitted with the Crystal Ball function.

4.3. Response to a head-on 14-MeV electron beam

Both, the PbGl and the PbF_2 detectors, showed clear signal peaks for 14-MeV electrons entering the front face of the radiators, well separated from the noise. Fig. 3 shows a comparison of the measured signals for the four different detector types and the corresponding simulated signals in number of p.e.

The measured signal heights were largest for PbF_2. Among the PbGl detectors of approximate the same shape and size, the type SF5 performed best. A beam-spot scan over the front faces of the radiators showed a large homogeneity of the response: Only very close to the edges a low-energy tail developed from the peak. The measured signals from a scan of the PbGl detector of type SF5 from the center of the radiator to a corner are shown in Fig. 4.

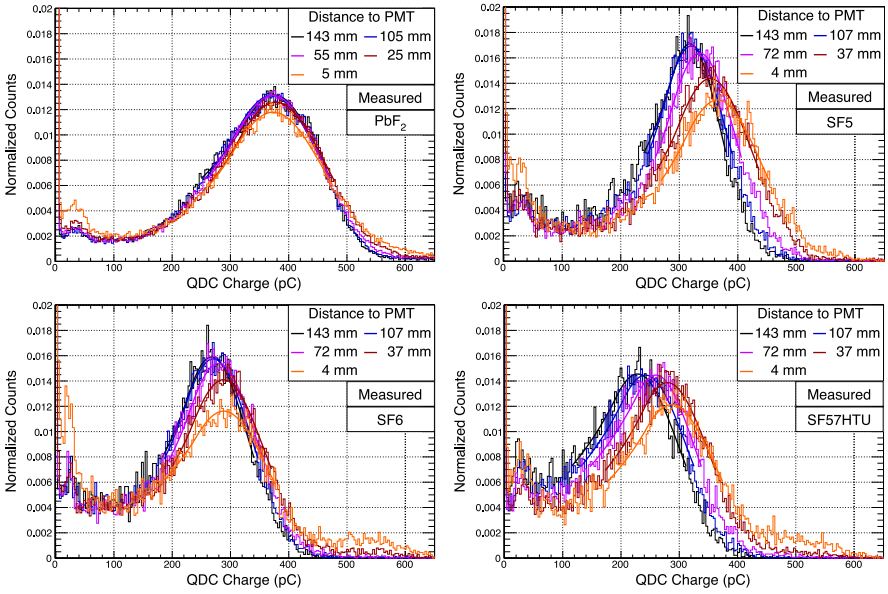

Fig. 5. Measured signals from PbF_2 (top left) and PbGl (top right SF5, bottom left SF6, bottom right SF57HTultra) detectors for a 14-MeV electron beam entering a side face of the detector at different distances (as shown in the legends) to the PMT face. The FWHM of the beam was $\varnothing_B \approx 41$ mm. The signal peaks were fitted with the Crystal Ball function.

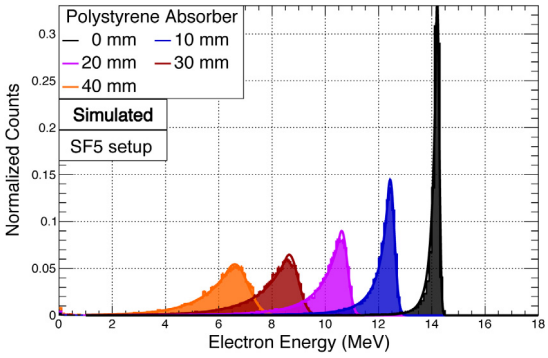

Fig. 6. Representative simulated energy distributions of the energy-degraded electron beam for polystyrene absorbers of thicknesses up to 40 mm. The beam left the vacuum beam pipe through an aluminum flange of 0.2 mm thickness followed by the energy-degraders and 270–320 mm of air, ~2.4 mm of plastic scintillator, and additional 72–115 mm of air before hitting the detectors. Variations with respect to the trigger conditions and the detector setup were found to be small. The signal peaks were fitted with the Crystal Ball function.

4.4. Response to a side-on 14-MeV electron beam

Beam-spot scans over the side faces of the detectors were used to study their response in comparison to a head-on beam. This is especially important for Cherenkov radiators as their light is emitted in forward direction with respect to the electrons. Fig. 5 shows the measured signals for a side-on 14-MeV electron beam hitting the detector at different distances to the PMT face. For the PbF_2 detector no significant difference to the response to a head-on beam was found, which is explained by the immediate wide-angle scattering of the 14-MeV electrons inside the dense material. In addition, a 45° incident beam angle was examined leading to the same result. For the PbGl detectors an increase (of approximately 25% in SF57HTultra and less in the other types) in signal height was found when approaching the PMT face. For these detectors the differences in geometry and optical properties were causing an increase of direct light reaching the PMT photocathode without reflections.

4.5. Response to an energy-degraded electron beam

With additional beam energy-degraders made from polystyrene absorbers ($[C_6H_5CHCH_2]_n$ with $\rho = 1.06$ g/cm^3 and $dE/dx|_{\text{min}} = 1.94$ MeV cm^2/g) of one to several cm thickness, the detector response was also studied for beam energies below 14 MeV down to approximately 6 MeV. The collisional energy loss in the absorber was approximately 0.21 MeV/mm. The simulated energy distributions of the beam for absorber thicknesses up to 40 mm are shown in Fig. 6, in which each incoming beam electron was tracked in the simulation from the vacuum beam pipe through all materials and its remaining energy was determined at the first interaction point in the detector. The fluctuations in energy-loss lead to the increasing energy spread for thicker absorbers with a relative energy spread σ_B/E_B of 0.5% at 14 MeV to 8% at 6 MeV. However, even after 40 mm thickness a very pronounced peak remains for electrons reaching the detectors. For all absorbers the beam energy spread σ_B was below 0.5 MeV, providing a sufficiently precise determination of the beam energy for the following studies.

A comparison of the observed to the simulated signals is shown in Fig. 7 for a PbF_2 detector. The simulation for the detector response to electrons of low energy provided a good description of the measurements in the signal peak region. The measurements for the three different types of PbGl detectors are shown in Fig. 8.

Using the simulated electron beam energies, the detector response function was then extracted from the data. Fig. 9 shows the measured and simulated signal heights for electrons of 6–14 MeV energy entering the front face of the radiators. The simulation shows a linear trend of signal height versus beam energy that is also observed in the data for beam energies above 10 MeV, demonstrating a good linearity of the measured energy response. Below this energy the beam degradation and energy straggling lead to small non-linear effects. Fig. 9 also provides the measured and simulated relative energy resolutions at the corresponding peak positions.

5. Discussion and outlook

A calibration of the measured spectra was performed to express the results in terms of p.e. and to provide more general information

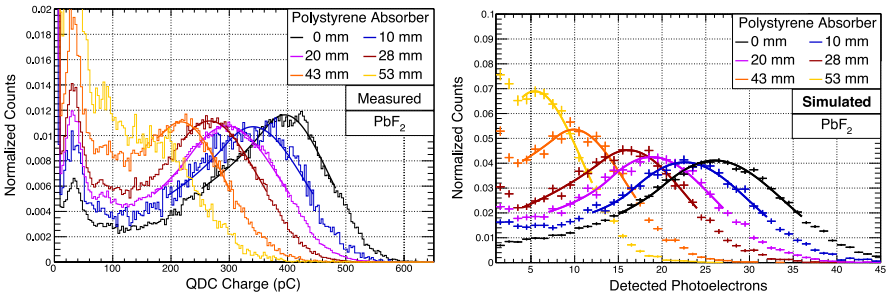

Fig. 7. Measured (left) and simulated (right) signals from a PbF_2 detector for electrons of 6–14 MeV energy entering the front face of the radiator. The signal peaks could be resolved even below 10 MeV and were fitted with the Crystal Ball function.

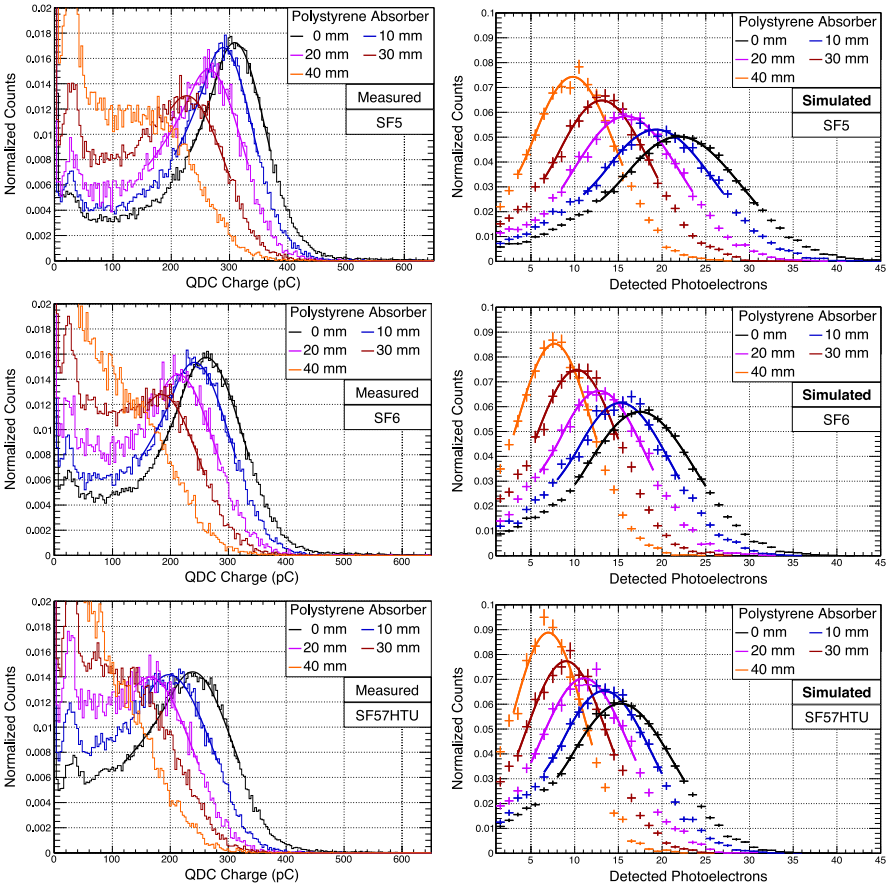

Fig. 8. Same as Fig. 7 but for PbGl detectors of type SF5 (top), SF6 (center), and SF57HTultra (bottom).

useful for other setups. Fig. 10 shows the measured versus the simulated peak positions in number of photoelectrons and a linear fit that yielded a calibration factor of 13.4 ± 0.8 pC/p.e. and small residuals that demonstrate the robustness of the calibration.

The response of several PbF_2 crystals and three types of PbGl blocks was measured with a 14-MeV MAMI beam during two beam-times in July and December 2018. The obtained results for different detector geometries were also compared to Monte Carlo simulations of energy-loss, light production, transport, and detection. A quantitative comparison of the response of the studied radiators is shown in Table 4. The measured signal height in PbF_2 after calibration was $N \sim 27$ p.e., corresponding to approximately 1.8 p.e. per MeV energy deposition. The lead glasses yielded between 1.0 and 1.5 p.e./ MeV. These numbers were in agreement with a simulation-independent estimate for which the measured relative peak width σ_E/E is related to a Poissonian distributed number of p.e. using the purely statistical assumption that the variance in the count equals the mean count, i.e. $\sigma_N/N = 1/\sqrt{N}$. For beam energies near 14 MeV the measured energy resolutions, corrected for the contribution from the relative beam energy spread, were found to be between 20% and 40%. The systematic uncertainties of these results were dominated by uncertainties in the calibration method.

Even though SF5 showed a lower transmittance compared to other PbGl variants with superior transmittance, the position and the slope of its UV absorption band between 330 and 370 nm is favorable for a Cherenkov radiator. In contrast, the UV absorption band in SF57HTultra between 360 and 390 nm hinders the emission of Cherenkov light. The type SF57HTultra showed the lowest performance

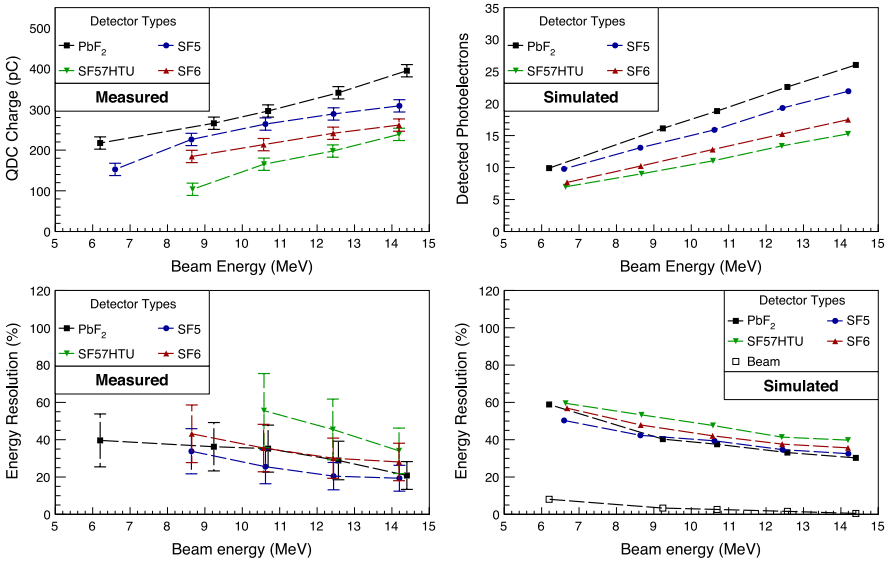

Fig. 9. Top: Measured (left) and simulated (right) signal heights for electrons of 6–14 MeV energy entering the front face of the radiators. The signal heights increase approximately linearly with energy. The materials PbF_2 and PbGl type SF5 yielded more light than the types SF6 and SF57HTultra. Bottom: Measured (left) and simulated (right) relative energy resolutions for these beam energies as determined by the width of the Gaussian component of the Crystal Ball function. The simulated contribution from the relative beam energy spread (shown with □ symbols) has been subtracted quadratically from the measured energy resolutions.

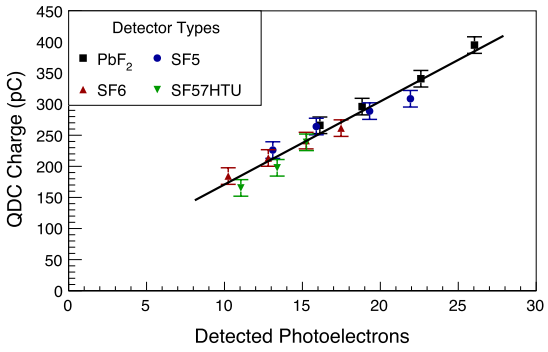

Fig. 10. Calibration of the measured signal heights in number of photoelectrons using the simulation. The linear fit yielded a calibration factor of 13.4 ± 0.8 pC/p.e. as well as small and randomly dispersed residuals.

in the beam-test. In conclusion, the beam-tests proofed the materials PbF_2 and SF5 PbGl to be well suited as calorimeter material in this energy range.

The motivation of this study was the verification of high-density Cherenkov radiators as calorimeter materials for energies near 10 MeV, where the possible detection of electrons recoiling off dark sector particles in the future beam-dump experiment DarkMESA can give stringent exclusion limits for dark photons [1]. A staged approach for DarkMESA is foreseen to increase its detector volume and mass within the next years. The simulation will allow to determine the optimal shape of the active volumes, the minimal energy threshold, and the detector efficiency. Design studies for the calorimeters are shown in Fig. 11. Stage A of DarkMESA will employ more than one thousand PbF_2 crystals and their PMTs of the former A4 experiment at MAMI for building a $1 \times 1 \times 0.13$ m^3 calorimeter with a mass of 1200 kg. This calorimeter will be arranged in sub-modules of 5×5 crystals, to be filled in a stainless steel grid with 20×20 cm^2 compartments. Each sub-module will cover an active volume of ~3200 cm^3 while weighting less than 50 kg. In a second stage, additional calorimeters will be constructed from PbGl blocks of type SF5, a first prototype with a volume of 0.04 m^3 and a mass of 150 kg is under development. In the current design the completed stage B calorimeters would comprise 1 m^3 volume and a mass of 4100 kg. The final stage C could contain a volume of up to 10 m^3. Alternatively, a calorimeter made from scintillating material such as CsI(Tl) or BGO could be constructed behind the Cherenkov light calorimeters. To explore the physics reach of the DarkMESA experiment, the reachable exclusion limits for detecting electrons recoiling from LDM particles were calculated for the staged calorimeter designs using the detector responses presented in this study [22].

CRediT authorship contribution statement

M. Christmann: Conceptualization, Methodology, Data curation, Formal analysis, Software, Writing - original draft, Review & editing. **P.F. Burger:** Conceptualization, Methodology, Data curation, Formal analysis, Software, Review & editing. **P. Achenbach:** Conceptualization, Methodology, Data curation, Formal analysis, Software, Funding acquisition, Project administration, Resources, Supervision, Writing - original draft, Review & editing. **S. Aulenbacher:** Conceptualization, Methodology, Data curation, Formal analysis, Software, Review & editing. **M. Ball:** Review & editing. **S. Baunack:** Conceptualization, Methodology, Data curation, Formal analysis, Software, Funding acquisition, Project administration, Resources, Supervision, Review & editing. **J.C. Bernauer:** Review & editing. **M. Biroth:** Conceptualization, Methodology, Data curation, Formal analysis, Software, Review & editing. **S. Caiazza:** Conceptualization, Methodology, Data curation, Formal analysis, Software, Review & editing. **E. Cline:** Review & editing. **A. Denig:** Conceptualization, Methodology, Data curation, Formal analysis, Software, Funding acquisition, Project administration, Resources, Supervision, Review & editing. **L. Doria:** Conceptualization, Methodology, Data curation, Formal analysis, Software, Funding acquisition, Project administration, Resources, Supervision, Writing - original draft, Review & editing. **I. Friščić:** Review & editing. **J. Geimer:** Conceptualization, Methodology, Data curation, Formal analysis, Software, Review & editing. **P. Gülker:** Conceptualization, Methodology, Data curation, Formal analysis, Software, Review & editing. **A. Khoukaz:** Review & editing. **M. Kohl:** Review & editing. **T. Kolar:** Review &

Table 4
Comparison of the response of PbF_2 and PbGl detectors to 14-MeV electrons entering the front face of the radiators. The table lists the signal height E, the Gaussian width of the signal peak at the high-energy side σ_E, the full width at half maximum of the signal peak FWHM before calibration, as well as the number of p.e., the signal height per MeV deposited energy $N/\Delta E$, and the relative energy resolution σ_N/N after calibration. The last column shows the relative energy resolution projected to 1 GeV energy-loss assuming the dominance of statistical fluctuations in the low-energy measurements.

Material	Measured data			Calibrated results			
	E (pC)	σ_E (pC)	FWHM (pC)	N (p.e.)	$N/\Delta E$ (p.e./MeV)	σ_N/N (%)	σ_N/N (%/$\sqrt{\Delta E}$ [GeV])
PbF_2	395	75	231	26.8 ± 1.8	1.8 ± 0.1	21 ± 7	2.5 ± 0.9
SF5	309	53	139	20.3 ± 1.5	1.5 ± 0.1	19 ± 7	2.3 ± 0.8
SF6	261	63	159	16.8 ± 1.4	1.2 ± 0.1	28 ± 10	3.3 ± 1.2
SF57HTU	239	69	200	15.1 ± 1.3	1.0 ± 0.1	34 ± 12	4.1 ± 1.5

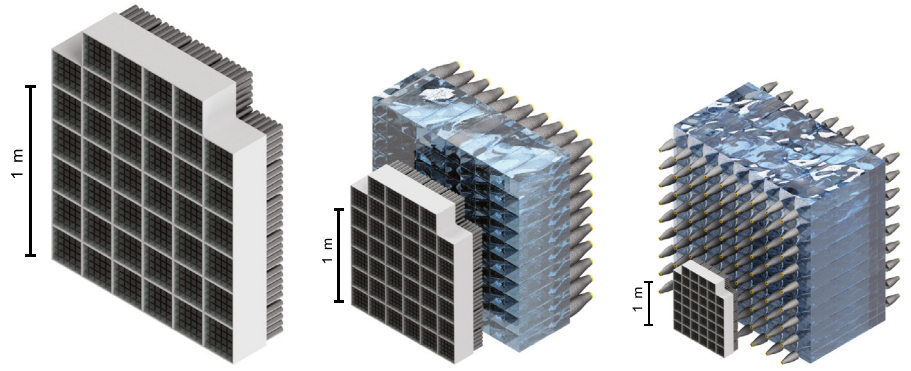

(a) *Stage A:* A forward wall of ≈ 1000 PbF_2 crystals with a volume of 0.13 m^3 and a mass of 1200 kg.

(b) *Stage B:* The PbF_2 wall and an additional block of PbGl with a volume of 1 m^3 and a mass of 4100 kg.

(c) *Stage C:* The PbF_2 wall and an additional block of PbGl with a possible volume of up to 10 m^3.

Fig. 11. Design studies for the DarkMESA detector. The calorimeters are segmented and smaller blocks will be read out by one PMT, while larger blocks will be read out by two PMTs.

editing. **M. Lauß:** Conceptualization, Methodology, Data curation, Formal analysis, Software, Review & editing. **W. Lauth:** Conceptualization, Methodology, Data curation, Formal analysis, Software, Funding acquisition, Project administration, Resources, Supervision, Review & editing. **M. Littich:** Conceptualization, Methodology, Data curation, Formal analysis, Software, Review & editing. **M. Lupberger:** Review & editing. **S. Lunkenheimer:** Conceptualization, Methodology, Data curation, Formal analysis, Software, Review & editing. **F.E. Maas:** Conceptualization, Methodology, Data curation, Formal analysis, Software, Funding acquisition, Project administration, Resources, Supervision, Review & editing. **M. Mauch:** Conceptualization, Methodology, Data curation, Formal analysis, Software, Review & editing. **H. Merkel:** Conceptualization, Methodology, Data curation, Formal analysis, Software, Funding acquisition, Project administration, Resources, Supervision, Review & editing. **M. Mihovilovič:** Review & editing. **R.G. Milner:** Review & editing. **J. Müller:** Conceptualization, Methodology, Data curation, Formal analysis, Software, Review & editing. **J. Rausch:** Conceptualization, Methodology, Data curation, Formal analysis, Software, Review & editing. **B.S. Schlimme:** Conceptualization, Methodology, Data curation, Formal analysis, Software, Funding acquisition, Project administration, Resources, Supervision, Review & editing. **C. Sfienti:** Conceptualization, Methodology, Data curation, Formal analysis, Software, Funding acquisition, Project administration, Resources, Supervision, Review & editing. **S. Širca:** Review & editing. **S. Stengel:** Conceptualization, Methodology, Data curation, Formal analysis, Software, Review & editing. **C. Szyszka:** Conceptualization, Methodology, Data curation, Formal analysis, Software, Review & editing. **S. Vestrick:** Review & editing. **Y. Wang:** Review & editing.

Acknowledgments

We would like to thank the MAMI operators, technical staff, and the accelerator group for their excellent support to perform the experiments with a high-precision electron beam.

This work was supported by the PRISMA and PRISMA$^+$ Clusters of Excellence "Precision Physics, Fundamental Interactions and Structure of Matter" and by the Helmholtz-Gemeinschaft Deutscher Forschungszentren (HGF) with a HGF-Exzellenznetzwerk.

Declaration of competing interest

The authors declare that they have no known competing financial interests or personal relationships that could have appeared to influence the work reported in this paper.

Appendix A. Detailed optical properties of PbF_2

See Fig. A.12.

Appendix B. Detailed optical properties of lead glasses

See Fig. B.13.

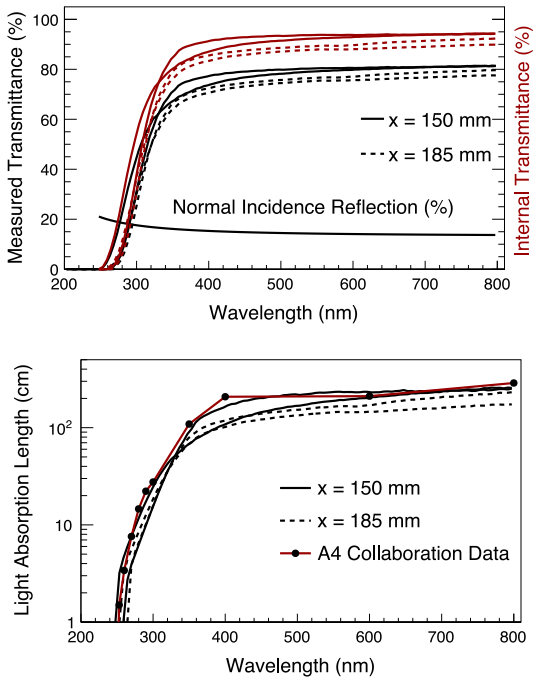

Fig. A.12. Top: Measured spectral transmittances τ and calculated internal transmittances $\tau_i = \tau/P$ for different PbF_2 crystals with two different lengths x. The complement of the reflection factor for normal incident light $(1-P)$, calculated from the Fresnel reflectivity considering multiple reflections, is indicated. Bottom: Comparison of the corresponding light absorption length $\Lambda_{\text{abs}} = -x/\ln(\tau_i)$ with data from the A4 Collaboration.

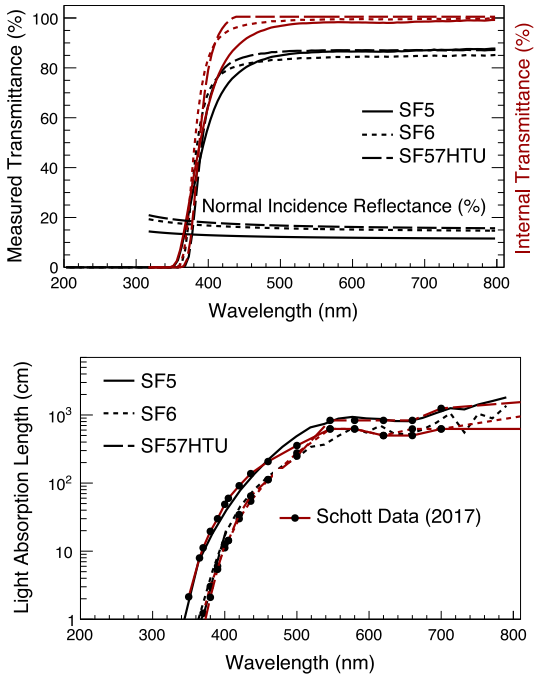

Fig. B.13. Top: Measured spectral transmittances τ and calculated internal transmittances $\tau_i = \tau/P$ for different PbGl blocks with different lengths x. The complement of the reflection factor for normal incident light $(1-P)$, calculated from the Fresnel reflectivity considering multiple reflections, is indicated. Bottom: Comparison of the corresponding light absorption length $\Lambda_{\text{abs}} = -x/\ln(\tau_i)$ with data from the manufacturer.

References

[1] L. Doria, P. Achenbach, M. Christmann, A. Denig, P. Gülker, H. Merkel, Search for light dark matter with the MESA accelerator, in: Proc. Thirteenth International Conference on the Intersection of Particle and Nuclear Physics (CIPANP18), Palm Springs, CA, United States, 29 May–3 June 2018, 2018, arxiv:1809.07168.

[2] L. Doria, P. Achenbach, M. Christmann, A. Denig, H. Merkel, Dark matter at the intensity frontier: The new MESA electron accelerator facility, in: Proc. Alpine LHC Physics Summit 2019 (ALPS 2019), Obergurgl, Austria, 22–27 Apr. 2019, 2019, arxiv:1908.07921.

[3] J.D. Bjorken, R. Essig, P. Schuster, N. Toro, New fixed-target experiments to search for dark gauge forces, Phys. Rev. D 80 (2009) 075018, http://dx.doi.org/10.1103/PhysRevD.80.075018.

[4] D. Becker, et al., The P2 experiment: A future high-precision measurement of the electroweak mixing angle at low momentum transfer, Eur. Phys. J. A 54 (2018) 208, http://dx.doi.org/10.1140/epja/i2018-12611-6.

[5] P. Lecoq, et al., Lead tungstate ($PbWO_4$) scintillators for LHC EM calorimetry, Nucl. Instrum. Methods Phys. Res. A 365 (1995) 291–298, http://dx.doi.org/10.1016/0168-9002(95)00589-7.

[6] J. Brose, G. Dahlinger, K.R. Schubert, Properties of CsI(Tl) crystals and their optimization for calorimetry of high-energy photons, Nucl. Instrum. Methods Phys. Res. A 417 (1998) 311–324, http://dx.doi.org/10.1016/S0168-9002(98)00765-7.

[7] B. Aubert, et al., (BaBar Collaboration), The BaBar detector, Nucl. Instrum. Methods Phys. Res. A 479 (2002) 1–116, http://dx.doi.org/10.1016/S0168-9002(01)02012-5.

[8] R. Sumner, (L3 Collaboration), The L3 BGO electromagnetic calorimeter, Nucl. Instrum. Methods Phys. Res. A 265 (1988) 252–257, http://dx.doi.org/10.1016/0168-9002(88)91078-9.

[9] F. Ferroni, The L3 BGO electromagnetic calorimeter at LEP, Nucl. Phys. B (Proc. Suppl.) 23 (1991) 100–106, http://dx.doi.org/10.1016/0920-5632(91)90036-E.

[10] M. Battaglieri, et al., Dark matter search in a Beam-Dump eXperiment (BDX) at Jefferson Lab, Proposal to the Program Advisory Committee 45, Thomas Jefferson Laboratory, 2018, http://dx.doi.org/10.2172/1431583.

[11] P. Gianotti, (PADME Collaboration), The calorimeters of the PADME experiment, Nucl. Instrum. Methods Phys. Res. A 936 (2019) 150–151, http://dx.doi.org/10.1016/j.nima.2018.09.058.

[12] D.F. Anderson, M. Kobayashi, C.L. Woody, Y. Yoshimura, Lead fluoride: An ultra-compact Cherenkov radiator for em calorimetry, Nucl. Instrum. Methods Phys. Res. A 290 (1990) 385–389, http://dx.doi.org/10.1016/0168-9002(90)90553-I.

[13] U. Buchner, J.P. Donker, B. Spaan, J. Spengler, G. Schweda, D. Wegener, W. Schmidt-Parzefall, Performance of a scintillating glass calorimeter for electromagnetic showers, Nucl. Instrum. Methods Phys. Res. A 272 (1988) 695, http://dx.doi.org/10.1016/0168-9002(88)90750-4.

[14] S. Baunack, D. Balaguer Ríos, L. Capozza, J. Diefenbach, R. Frascaria, B. Gläser, D. von Harrach, Y. Imai, R. Kothe, R. Kunne, J.H. Lee, F.E. Maas, M.C. Mora Espí, M. Morlet, S. Ong, E. Schilling, J. van de Wiele, C. Weinrich, (A4 Collaboration), Real-time calibration of the A4 electromagnetic lead fluoride (PbF_2) calorimeter, Nucl. Instrum. Methods Phys. Res. A 640 (2011) 58–68, http://dx.doi.org/10.1016/j.nima.2011.02.099.

[15] P. Achenbach, I. Altarev, K. Grimm, T. Hammel, D. von Harrach, J. Hoffmann, H. Hofmann, E.-M. Kabuß, S. Köbis, A. Lopes-Ginja, F.E. Maas, H. Ströher, Radiation resistance and optical properties of lead fluoride Cherenkov crystals, Nucl. Instrum. Methods Phys. Res. A 416 (1998) 357–363, http://dx.doi.org/10.1016/S0168-9002(98)00748-7.

[16] P. Achenbach, S. Baunack, K. Grimm, T. Hammel, D. von Harrach, A. Lopes-Ginja, F.E. Maas, E. Schilling, H. Ströher, Measurements and simulations of Cherenkov light in lead fluoride crystals, Nucl. Instrum. Methods Phys. Res. A 465 (2001) 318–328, http://dx.doi.org/10.1016/S0168-9002(01)00668-4.

[17] K.-H. Kaiser, et al., The 1.5 GeV harmonic double-sided microtron at Mainz University, Nucl. Instrum. Methods Phys. Res. Sect. A 593 (2008) 159–170, http://dx.doi.org/10.1016/j.nima.2008.05.018.

[18] A.T. Fienberg, L.P. Alonzi, A. Anastasi, R. Bjorkquist, D. Cauz, R. Fatemi, C. Ferrari, A. Fioretti, A. Frankenthal, C. Gabbanini, L.K. Gibbons, K. Giovanetti, S.D. Goadhouse, W.P. Gohn, T.P. Gorringe, D.W. Hertzog, M. Iacovacci, P. Kammel, J. Kaspar, B. Kiburg, L. Li, S. Mastroianni, G. Pauletta, D.A. Peterson, D. Počˇ, M.W. Smith, D.A. Sweigart, V. Tishchenko, G. Venanzoni, T.D. Van Wechel, K.B. Wall, P. Winter, K. Yai, Studies of an array of PbF_2 cherenkov crystals with large-area sipm readout, Nucl. Instrum. Methods Phys. Res. A 783 (2015) 12–21, http://dx.doi.org/10.1016/j.nima.2015.02.028.

[19] A. Frankenthal, J. Alexander, B. Buonomo, E. Capitolo, C. Capoccia, C. Cesarotti, R.D. Sangro, C.D. Giulio, F. Ferrarotto, L. Foggetta, G. Georgiev, P. Gianotti, M. Hunyadi, V. Kozhuharov, A. Krasznahorkay, E. Leonardi, G. Organtini, G. Piperno, M. Raggi, C. Rella, A. Saputi, I. Sarra, E. Spiriti, C. Taruggi, P. Valente, Characterization and performance of PADME's Cherenkov-based small-angle calorimeter, Nucl. Instrum. Methods Phys. Res. A 919 (2019) 89–97, http://dx.doi.org/10.1016/j.nima.2018.12.035.

[20] Schott, Optical Glass: Data Sheets, Mainz, Germany, 2017. URL https://www.schott.com/advanced_optics/us/abbe_datasheets/schott-datasheet-all-us.pdf.

[21] M.J. Weber, Handbook of optical materials, CRC Press, Boca Raton, FL, United States, 2003.

[22] M. Christmann, P. Achenbach, S. Baunack, P. Burger, A. Denig, L. Doria, F. Maas, H. Merkel, Instrumentation and optimization studies for a beam dump experiment (BDX) at MESA — DarkMESA, in: Proc. 15th Vienna Conference on Instrumentation (VCI2019), Vienna, Austria, 18–22 Feb. 2019, Nucl. Instrum. Methods Phys. Res. A (2019) 162398, http://dx.doi.org/10.1016/j.nima.2019.162398.